HAL open science

Immunocytochemical Localization and Crystal Structure of Human Frequenin (Neuronal Calcium Sensor 1)

Yves Bourne, Jens Dannenberg, Verena Pollmann, Pascale Marchot, Olaf Pongs

To cite this version:

Yves Bourne, Jens Dannenberg, Verena Pollmann, Pascale Marchot, Olaf Pongs. Immunocytochemical Localization and Crystal Structure of Human Frequenin (Neuronal Calcium Sensor 1). Journal of Biological Chemistry, 2000, 276, pp.11949 - 11955. 10.1074/jbc.m009373200 . hal-03263149

HAL Id: hal-03263149

https://amu.hal.science/hal-03263149

Submitted on 17 Jun 2021

HAL is a multi-disciplinary open access archive for the deposit and dissemination of scientific research documents, whether they are published or not. The documents may come from teaching and research institutions in France or abroad, or from public or private research centers.

L'archive ouverte pluridisciplinaire **HAL**, est destinée au dépôt et à la diffusion de documents scientifiques de niveau recherche, publiés ou non, émanant des établissements d'enseignement et de recherche français ou étrangers, des laboratoires publics ou privés.

Distributed under a Creative Commons Attribution 4.0 International License

THE JOURNAL OF BIOLOGICAL CHEMISTRY
Vol. 276, No. 15, Issue of April 13, pp. 11949–11955, 2001
Printed in U.S.A.
© 2001 by The American Society for Biochemistry and Molecular Biology, Inc.

Immunocytochemical Localization and Crystal Structure of Human Frequenin (Neuronal Calcium Sensor 1)*

Received for publication, October 13, 2000, and in revised form, November 20, 2000
Published, JBC Papers in Press, November 22, 2000, DOI 10.1074/jbc.M009373200

Yves Bourne‡§¶, Jens Dannenberg§‖, Verena Pollmann‖, Pascale Marchot, and Olaf Pongs‖**

*From the ‡Architecture et Fonction des Macromolécules Biologiques, CNRS UMR-6098, 13402, Marseille Cedex 20, France, the ‖Universitaet Hamburg, Zentrum für Molekulare Neurobiologie, Institut für Neurale Signalverarbeitung, D20249 Hamburg, Germany, and the **Ingénierie des Protéines, CNRS UMR-6560, Institut Fédératif de Recherche Jean Roche, Université de la Méditerranée, 13916 Marseille Cedex 20, France*

Frequenin, a member of a large family of myristoyl-switch calcium-binding proteins, functions as a calcium-ion sensor to modulate synaptic activity and secretion. We show that human frequenin colocalizes with ARF1 GTPase in COS-7 cells and occurs in similar cellular compartments as the phosphatidylinositol-4-OH kinase PI4K*β*, the mammalian homolog of the yeast kinase PIK1. In addition, the crystal structure of unmyristoylated, calcium-bound human frequenin has been determined and refined to 1.9 Å resolution. The overall fold of frequenin resembles those of neurocalcin and the photoreceptor, recoverin, of the same family, with two pairs of calcium-binding EF hands and three bound calcium ions. Despite the similarities, however, frequenin displays significant structural differences. A large conformational shift of the C-terminal region creates a wide hydrophobic crevice at the surface of frequenin. This crevice, which is unique to frequenin and distinct from the myristoyl-binding box of recoverin, may accommodate a yet unknown protein ligand.

Frequenin (Frq),[1] or neuronal calcium-sensor 1, is a member of a family of related calcium-myristoyl-switch proteins that have been proposed to function as calcium-ion sensors. Members of this family include recoverin, GCAP, neurocalcin, visinin, and others (1). Recoverin and GCAP have been implicated in the control of recovery and adaptation in visual signal transduction. In vertebrate rod outer segments, GCAP apparently inhibits guanylate cyclase when the cytosolic concentration of Ca^{2+} is high in the dark, whereas recoverin may inhibit rhodopsin kinase (2, 3). Lowering the cytosolic Ca^{2+} during light illumination attenuates the inhibitory activities of GCAP and recoverin, leading to an activation of these enzymes.

Frq, on the other hand, has attracted much attention because it may function as a calcium-ion sensor to modulate synaptic activity and secretion (4–7). *Drosophila* Frq has been implicated in the facilitation of neurotransmitter release at neuromuscular junctions of third instar larvae *(Drosophila melanogaster). Drosophila* mutants that overexpress Frq show a facilitated neurotransmitter release that dramatically depend on the frequency of stimulation (4). Similarly, overexpression of a rat homolog of Frq in PC12 cells evokes an increased release of growth hormone in response to agonists like ATP (5). These results are consistent with the idea that Frq activity and regulated secretion are coupled.

More recently, it has been shown that the yeast homolog of Frq functions as a Ca^{2+}-sensing subunit of the yeast phosphatidylinositol (PtdIns)-4-OH kinase, PIK1, a key enzyme in the phosphoinositide signaling system (6). In *Saccharomyces cerevisiae*, PIK1 participates in the mating pheromone-signal transduction cascade and regulates secretion at the Golgi. PIK1 is essential in yeast cells for normal secretion, Golgi and vacuole membrane dynamics, and endocytosis (7). Yeast $PIK1^{ts}$ mutants exhibit severe protein trafficking defects and accumulate morphologically aberrant Golgi membranes (8). The aberrant Golgi morphology is strikingly similar to that found in yeast cells lacking a functional ARF1 GTPase (7). ARF1 has been implicated in multiple membrane trafficking events including the recruitment of the mammalian PIK1 homolog, PI4K*β*, to the Golgi membrane (9).

Here we show that human Frq (HuFrq) colocalizes with ARF1 in COS-7 cells and occurs in similar cellular localizations as PI4K*β*. In addition, in a further step toward understanding the cellular function of Frq, we report the crystal structure of unmyristoylated Ca^{2+}-bound human Frq (HuFrq) refined to 1.9 Å resolution. This structure confirms that frequenins belong to the large family of myristoyl-switch Ca^{2+}-binding proteins and reveals the architecture of the Ca^{2+}-binding sites. Most importantly, comparative analysis of the HuFrq structure with those of neurocalcin and recoverin highlights a unique wide crevice and a solvent-exposed carboxyl terminus that could be responsible for ligand recognition and account for the broad substrate specificity among members of the family.

EXPERIMENTAL PROCEDURES

HuFrq Cloning, Expression, and Purification—Human poly(A)RNA was isolated from HEK293 cells using the Fast Track II Kit (Invitrogen), and cDNA was synthesized with Superscript II Reverse Transcriptase (Life Technologies, Inc.). The HuFrq-encoding cDNA was amplified in a polymerase chain reaction (PCR) using *Pfu*Turbo-Polymerase (Life Technologies, Inc.) with the first strand cDNA as template and the primers 5′-ATACCATGGGGAAATCCAACAG-3′ (sense) and 5′-CTATACCAGCCCGTCGTAGAGG-3′ (antisense). Primer sequences were derived from the *HuFrq* nucleotide sequence

* This work was supported by the Deutsche Forschungsgemeinschaft (SFB 444-B4, to O. P.). The costs of publication of this article were defrayed in part by the payment of page charges. This article must therefore be hereby marked "*advertisement*" in accordance with 18 U.S.C. Section 1734 solely to indicate this fact.

The atomic coordinates and structure factors (code 1G8I) have been deposited in the Protein Data Bank, Research Collaboratory for Structural Bioinformatics, Rutgers University, New Brunswick, NJ (http://www.rcsb.org/).

§ These authors contributed equally to this work.

¶ To whom correspondence should be addressed. Tel.: 33-4-91-16-45-08; Fax: 33-4-91-16-45-36; E-mail: yves@afmb.cnrs-mrs.fr.

[1] Frq, frequenin; NCS-1, neuronal sensor 1; PAGE, polyacrylamide gel electrophoresis; PCR, polymerase chain reaction; RT-PCR, reverse transcription-PCR; TGN, trans-Golgi-network; MALDI-TOF, matrix-assisted laser desorption ionization time-of-flight mass spectrometry; HEK, human embryonic kidney cells; r.m.s.d., root mean square deviation; PIK1, yeast phosphatidylinositol-4-OH kinase; PI4K*β*, mammalian homolog of phosphatidylinositol-4-OH kinase.

This is an Open Access article under the CC BY license.

(GenBank™/EBI accession no. AF186409). The restriction sites *Nco*I and *Nde*I were used for subcloning into expression vector pET-16b (Promega) to generate expression plasmid pET-HuFrq. All nucleotide sequences were verified by automated sequencing.

The expression plasmid pET-HuFrq was transformed into *Escherichia coli* strain BL21(DE3) (Novagen). Transformed cells were grown in Luria-Bertani (LB) medium containing ampicillin (100 μg/ml) at 37 °C. HuFrq expression was induced overnight at an A_{600} of 0.8 with 0.5 mM isopropyl-1-thio-β-D-galactopyranoside and reached average yields of 20 mg/liter. Cells were harvested by centrifugation, resuspended in 20 ml of lysis buffer (50 mM HEPES, pH 7.4; 100 mM KCl; 1 mM EGTA; 1 mM dithiothreitol; 1 mM $MgCl_2$) per 1 liter medium, and lysed in a French pressure cell. Protamine sulfate was added to a final concentration of 0.1% for 10 min and then the lysate was cleared by centrifugation (40,000 × *g*, 30 min, 4 °C). The supernatant was filtered (0.45 μm), adjusted to 1 mM $CaCl_2$, and applied to a 15-ml phenyl-Sepharose CL4-B column (Amersham Pharmacia Biotech). The column was washed with buffer A (20 mM Tris/HCl, pH 7.9; 1 mM $MgCl_2$; 1 mM dithiothreitol) containing 1 mM $CaCl_2$ until A_{280} was below 0.01, and then the protein was eluted with buffer A containing 2 mM EGTA. The eluate was applied to a 3-ml HiTrapQ column (Amersham Pharmacia Biotech). The column was washed with buffer A containing 60 mM NaCl and 1 mM $CaCl_2$, and eluted with 120 mM NaCl in buffer A. The HuFrq-containing fractions were extensively dialyzed against water and concentrated to 10 mg/ml using microconcentrators (Pall Filtron). MALDI-TOF analysis of the purified HuFrq used the linear mode and a 337-nm nitrogen laser (Voyager-DE™RP BioSpectrometer work station, Perseptive Biosystems).

Site-directed Mutagenesis—Point mutations into *Frq* cDNA were introduced by PCR using the following mutation primers: 5′-GGCAGGATCGTGTTCTCCGAATTC-3′ and 5′-TCGGAGAA CACGATCCTGCCAT-3′ for E81V (EF2); 5′-ACATCGCCAG AAACGAGATGCTG-3′ and 5′-CTGGTTTCTGC CGATGTAGCCGTC-3′ for T117A (EF3); 5′-GGGAAGCTAGCTCTTCAGGAGTTC-3′ and 5′-CCTGAAGAGCTAGCTTCCCATCA-3′ for T165A (EF4). PCR fragments were cloned into pET16b and sequenced before use.

^{45}Calcium Binding Assay—Protein samples were resolved by SDS-polyacrylamide gel electrophoresis and transferred to nitrocellulose. The $^{45}Ca^{2+}$ blotting was performed as previously described (10); autoradiographic exposure time was 2 days.

Immunofluorescence Microscopy—The polyclonal anti-HuFrq antibodies were raised in rabbit against purified HuFrq and purified by affinity chromatography on HuFrq-Sepharose 4B according to the manufacturer's instructions (Amersham Pharmacia Biotech); specificity analyses performed by enzyme-linked immunosorbent assay showed full recognition of the immunizing HuFrq but no recognition of either recoverin or neurocalcin (11). COS-7 cells were cultured at 37 °C in Dulbecco's modified Eagle's medium (Life Technologies) supplemented with 10% (v/v) fetal calf serum (Life Technologies). They were grown to 60% confluency on poly-L-lysine-coated glass-coverslips. The cells were fixed with 4% (v/v) paraformaldehyde in phosphate-buffered saline for 15 min at room temperature, washed twice with phosphate-buffered saline and blocked with 1% (v/v) goat serum and 1% (w/v) bovine serum albumin in phosphate-buffered saline. Permeabilization used a blocking solution containing 0.3% (v/v) Triton X-100. Successive incubations with primary and secondary antibodies were carried out for 1 h at room temperature. Cells were washed in phosphate-buffered saline, and coverslips were mounted with Fluoromount GC (Southern Technologies). The cells were visualized and confocal images acquired using a confocal laser scanning microscope (Leica TCS NT). Primary antibodies were detected by species-specific cyanine dye-conjugated secondary antibodies (Jackson ImmunoResearch Laboratories): Cy3-conjugated antibodies were used for visualization of anti-HuFrq and anti-PI4Kβ (Upstate Biotechnology) staining, whereas Cy2- and Cy5-conjugated antibodies were used for anti-γ-adaptin (Sigma) and anti-ARF1 (Santa Cruz Biotechnology) staining, respectively.

Crystallization and Data Collection—Crystals were obtained at 4 °C using the vapor diffusion technique. Typically, 5 μl of the HuFrq solution were mixed with 5 μl of a reservoir solution made of 0.1 M sodium cacodylate, pH 6.5, 0.2 M NaAc, 30% polyethylene glycol M_r 8,000 (Crystal Screen I, solution 28, Hampton Research). Under rare circumstances, three different crystal forms grew from this solution: needle-like (form A), thin plates (form B), and thick plates (form C). Form A crystals belong to the hexagonal space group $P6_{1/5}$ with unit cell dimensions: $a = b = 82.2$ Å and $c = 56$ Å and contains one HuFrq molecule per asymmetric unit. Both form B and C crystals belong to the monoclinic space group $P2_1$ with unit cell dimensions: $a = 53.8$ Å, $b = 55.5$ Å, $c = 77.7$ Å, $\beta = 107.6°$, and $a = 29.6$ Å, $b = 105.2$ Å, $c = 55.2$ Å, $\beta = 106.6°$, respectively, and contain two HuFrq molecules per asymmetric unit. Crystals selected for data collection were briefly soaked into the reservoir solution supplemented with 10% (v/v) ethylene glycol, flash-cooled at 100 K in the nitrogen gas stream and stored in liquid nitrogen. No single crystal could be selected for form C. Data for forms A and B were collected on beamline ID14-EH2 of ESRF (Grenoble, France). Oscillation images were integrated with DENZO (12) and scaled and merged with SCALA (13). Amplitude factors were generated with TRUNCATE (13). Form A crystals were found to be twinned and the collected data could not be used.

TABLE I
Data collection and refinement

Crystal form	B
Resolution (Å)	1.9
No. observations	281,683
No. unique	35,881
R_{sym}[a] (%)	6.0 (35)
I/σ(I)	8.9 (2.0)
Redundancy	3.3
Completeness (%)	99 (98.9)
Resolution (Å)	20–1.9
R-factor[b] − *R* free (%)	22–25.6
No. of reflections (no σ cutoff)	35,849
Rms deviations	
bond length (Å)	0.016
bond angles (°)	1.7
dihedral angles (°)	21.3
improper angles (°)	1.2
Mean B factors (Å^2)	
main/side chain	26/30
solvent/Ca^{2+}	34/22
Rms deviations on B factors (Å^2)	
main chain	1.6
side chain	2.3

[a] $R_{sym} = |I - \langle I\rangle|\langle I\rangle$, where I is intensity and $\langle I\rangle$ is the average I for all observations of equivalent reflections. Values in brackets are for the outer resolution shell.

[b] *R*-factor = $|F_{obs}| - |F_{calc}|/|F_{obs}|$. *R*-free same as *R*-factor for 2% of the data omitted from the refinement.

Structure Determination and Refinement—Initial phases for form B crystals were obtained by molecular replacement using the structure of neurocalcin (14) (PDB code 1BJF) as a search model with the AMoRe package (15), giving a correlation coefficient of 36% and an *R*-factor value of 48% in the 15 to 4 Å resolution range. Rigid-body refinement, performed on each molecule with CNS (16) using data between 20 and 3 Å, gave an *R*-factor of 49%. For 2% of the reflections against which the model was not refined, *R*-free was 48%. The model was refined to 1.9 Å resolution using CNS, including bulk solvent and anisotropic B-factor corrections; the resulting 2Fo-Fc and Fo-Fc electron density maps were used to correct the model with the graphics program TURBO-FRODO (17). Solvent molecules automatically added using CNS were carefully examined on the graphics display. The final model comprises residues Asn^5–Val^{190} and Asn^5–Gly^{188}, respectively, for the two molecules in the asymmetric unit. High temperature factors and weak electron density are associated with residues 1–7, 49–60, and 133–138. The average r.m.s.d. between the two HuFrq molecules is 0.6 Å for 182 Cα atoms with the largest deviation (1.4 Å) for residue Gln^{54}. The stereochemistry of the model was analyzed with PROCHECK (18); no residues were found in the disallowed regions of the Ramachandran plot. Data collection and refinement statistics are summarized in Table I. The coordinates and structure factors of HuFrq have been deposited with the Protein Data Bank (1G8I). Fig. 1*B* was generated by ALSCRIPT (19) and Figs. 4–5 with SPOCK (20) and Raster3D (21).

RESULTS AND DISCUSSION

Chromosomal Localization—A search in the HTGS data bank with the *HuFrq* cDNA sequence revealed that the *HuFrq* gene is located on chromosome 9. A comparison of the publicly available chromosome 9 DNA sequence with the frequenin cDNA sequence showed that the exon-intron organization between *Drosophila* (4) and *HuFrq* genes has been conserved. Both open reading frames are interrupted by the same exon-intron borders and each are composed of same 8 exons (Fig. 1*A*). About 50 kilobases upstream of the first Frq

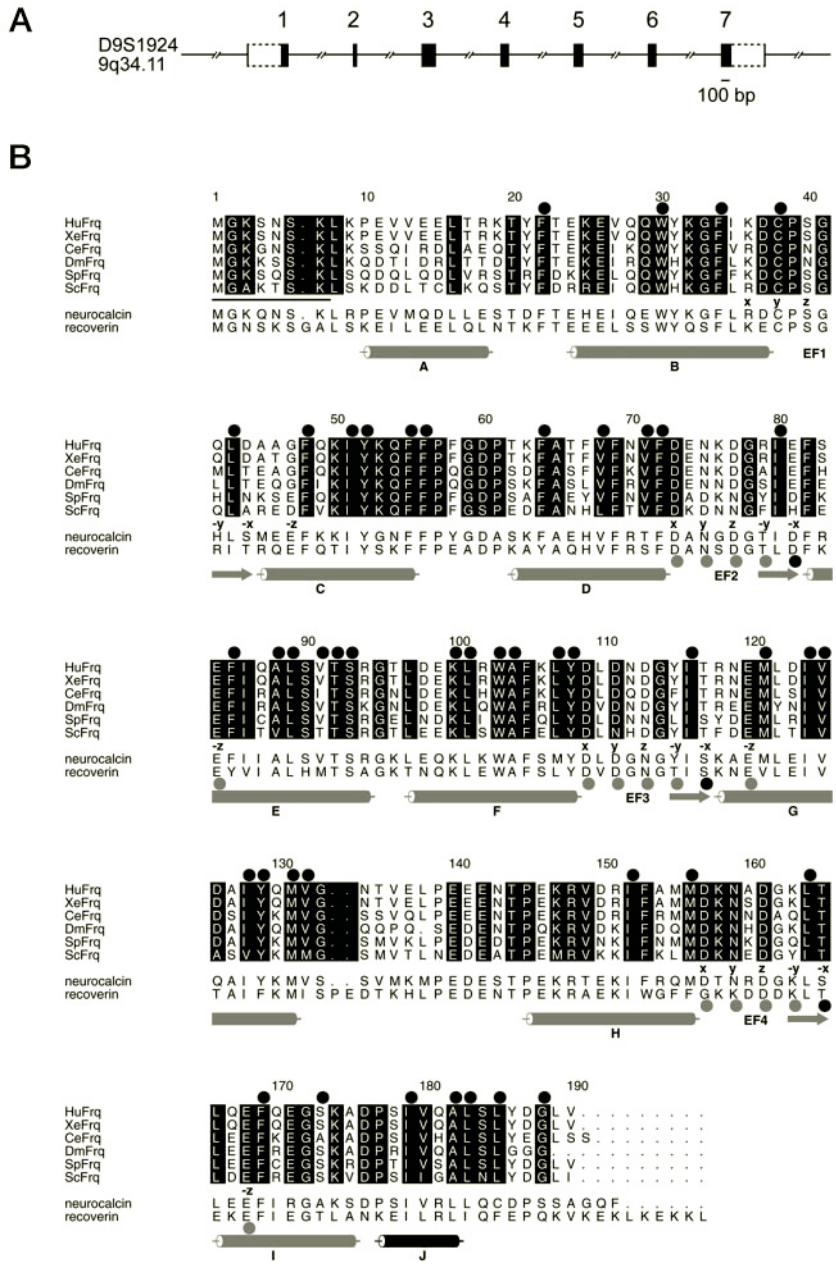

FIG. 1. **Exon-intron map of the *HuFrq* gene and sequence.** *A, black boxes* correspond to the open reading frame and *broken lines* to introns. Because the available genomic DNA sequence data of the *HuFrq* gene are not contiguous, exact sizes of introns are not known. Likewise, the 5′- and 3′-ends of *Hufrq* mRNA have not been mapped. Exons are drawn to scale as indicated by the *bar*. Exons 1 and 7 may contain untranslated sequence as indicated by *dotted lines*. The open reading frame in the first exon starts at nucleotide 155870 of the genomic clone AC006241. The STS marker D9S1924 is located at map position 9q34.11 corresponding to nucleotides 121075–121194. *B,* amino acid sequence alignment of HuFrq with homologous proteins. Invariant residues within HuFrq are highlighted in *white* with a *black background*. The secondary structural elements are shown in *gray* with the four EF hands labeled EF1 to EF4. Ca^{2+}-bound residues are indicated by *gray dots* and residues that are solvent exposed in the crevice by *black dots*. The N-terminal myristoylation site is *underlined*, and the mutated residues are indicated with *black dots*.

exon are located several STS markers, *e.g.* DGS1924, A001W37, STSG22304, placing the *Frq* gene at 9q34.11. To our knowledge, a human disease has not been associated yet with this locus.

Molecular Identification and Immunocytochemical Localization—Previously, mammalian homologs of *Drosophila* Frq have been cloned (22, 23). We have used this information to clone HuFrq from human first strand cDNA (Fig. 1*A*). The predicted HuFrq sequence contains 190 amino acids (Fig. 1*B*) with a theoretical monoisotopic mass of 21,865.91 and exhibits four EF hand motifs that represent potential Ca^{2+}-binding domains. In HuFrq, as in other members of the family, the first of the four EF hand motifs is not likely to be a functional Ca^{2+}-binding site as it lacks two Ca^{2+}-coordinating amino acids. The HuFrq N terminus contains the consensus sequence MG*XXX*(S/T)K for myristoylation (24); hence it could be myristoylated like the rat homolog (5). The HuFrq sequence is 100% homologous to those of rat (5) and mouse (23) and it differs by a single amino acid from that of *Xenopus* (25). Remarkably, the yeast (6) and HuFrq protein sequences also show a high degree of conversation: 143 of 190 amino acids (75%) are either identical or correspond to conservative replacements (Fig. 1*B*).

In yeast, Frq has been shown to stimulate the activity of the PtdIns-4-OH kinase PIK1 (6), an enzyme that is essential for normal secretion, Golgi and vacuole membrane dynamics, and endocytosis (7). *Xenopus* Frq rescues a yeast Frq deletion mutant, indicating that Frq from higher eukaryotes is able to fulfill similar functions like yeast Frq (25). Consistent with the functional role of Frq in yeast are the phenotypes that have been described for *Drosophila* mutants (4) and for mammalian cells overexpressing Frq (5). In both cases, it appears that evoked secretion is stimulated by Frq (26).

The activity of PI4Kβ, the likely mammalian homolog of yeast PIK1 (26), is recruited by the small GTPase ARF1 to the Golgi and contributes to the regulation of Golgi membrane dynamics and Golgi-dependent vesicle formation (9). Accordingly, in immunocytochemical experiments we have compared the immunostaining patterns obtained with anti-PI4Kβ, anti-ARF1, and anti-HuFrq antibodies, respectively; overlapping

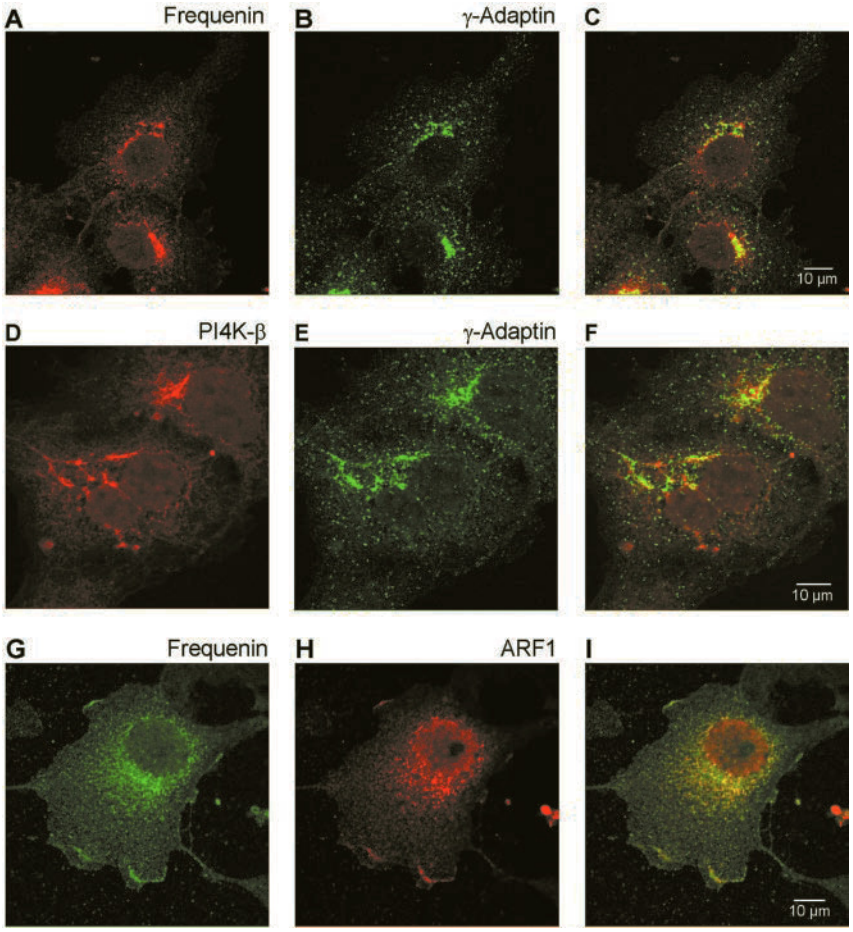

FIG. 2. **Immunocytofluorescent localization of HuFrq in COS-7 cells.** COS-7 cells were double stained with anti-HuFrq (*A*) and anti-γ-adaptin antibodies (*B*). Anti-HuFrq was detected by Cy3-conjugated goat anti-rabbit antibodies and anti-γ-adaptin by Cy2-conjugated goat anti-mouse antibodies. *C,* confocal microscopy emphasizing the colocalization of HuFrq and the Golgi marker γ-adaptin (*D–F*). COS-7 cells were double stained with anti-PIK4β (*D*) and anti-γ-adaptin antibodies (*E*). Anti-PIK4β was detected by Cy3-conjugated goat anti-rabbit antibodies and anti-γ-adaptin as in *B*. *F,* confocal microscopy emphasizing the colocalization of γ-adaptin and PIK4β. *G–I*, COS-7 cells were double stained with anti-HuFrq (*G*) and anti-ARF1 antibodies (*H*). Anti-HuFrq was detected as in A and anti-ARF1 by Cy5-conjugated mouse anti-goat antibodies. *I,* confocal microscopy emphasizing the colocalization of HuFrq and ARF1. *Scale bars* in C, F, and I are representative for all images shown at same magnification.

immunostaining reactions were observed (Fig. 2). For comparison, we also included in our investigations experiments with anti-γ-adaptin antibodies, a typical trans-Golgi network (TGN) marker. Paraformaldehyde-fixed COS-7 cells were first incubated with primary antibodies, *e.g.* polyclonal anti-HuFrq rabbit antibodies, monoclonal anti-γ-adaptin mouse antibodies, polyclonal anti-PI4Kβ rabbit antibodies, and polyclonal anti-ARF1 goat antibodies, respectively. Then, we used secondary Cy2-, Cy3-, or Cy5-labeled antibodies for immunocytofluorescent staining and localization of γ-adaptin, HuFrq and PI4Kβ, and ARF1, respectively, using confocal microscopy (Fig. 2). The anti-HuFrq antibodies revealed a pattern with a crescent of staining on one side of the nucleus and some punctuate staining within the cytoplasm (Fig. 2*A*). Staining could be eliminated by preincubation of the primary antibody with the immunizing HuFrq protein (not shown), indicating that the observed immunofluorescence is generated by HuFrq-specific antibodies. A similar staining pattern was obtained with γ-adaptin (Fig. 2*B*), which in double-labeling experiments colocalized with the HuFrq-immunostaining pattern (Fig. 2*C*). Previously, γ-adaptin has been shown to be localized in the TGN and the late endosomes (27). The double-immunostaining patterns also indicate a colocalization for γ-adaptin and PI4Kβ (Fig. 2, *D–F*) in agreement with a recent report (28). Finally, we coimmunostained the COS-7 cells with anti-HuFrq and anti-ARF1 antibodies (Fig. 2, *G–I*). Again, we observed a crescent of staining on one side of the nucleus (presumably the TNG) and some punctuate immunostain extending to the plasma membrane, which colocalized with the HuFrq immunostain (Fig. 2*I*). The results indicate similar subcellular distributions for HuFrq, ARF1, and PI4Kβ. The colocalization is consistent with the proposal that frequenin proteins modulate PtdIns-4-OH kinase activity both in yeast and in mammalian cells and thus may have similar regulatory functions in secretion and Golgi membrane dynamics.

Calcium-binding Properties—We mutated EF hands EF2, EF3, and EF4 of HuFrq together or in pairwise combinations utilizing *in vitro* mutagenesis. In all four cases, we mutated the amino acid residues at the -*X* position as previously described for *Drosophila* Frq (Fig. 1*B*) (4). Accordingly, we generated four HuFrq mutants: E81V/T117A/T165A ($Frq^{2,3,4}$), E81V/T117A ($Frq^{2,3}$), E81V/T165A ($Frq^{2,4}$), and T117A/T165A ($Frq^{3,4}$). Bacterial lysates containing approximately equal amounts of each HuFrq mutant were blotted onto nitrocellulose. The blot was incubated with $^{45}Ca^{2+}$ to investigate the Ca^{2+}-binding capacity of the HuFrq mutants in comparison to wild-type HuFrq (Fig. 3). The results showed that wild-type HuFrq yielded the highest $^{45}Ca^{2+}$ signal. We noted for the recombinant HuFrq mutants with pairwise mutations attenuated $^{45}Ca^{2+}$-signals of comparably reduced intensity. The pairwise HuFrq mutants each contained a single intact EF hand (EF2 in $Frq^{3,4}$, EF3 in $Frq^{2,4}$, and EF4 in $Frq^{2,3}$), yet they bound Ca^{2+} with high affinity; this suggests that EF hands EF2, EF3, and EF4 not only are functional in HuFrq but also are independent from each other. Previously, it was shown that single mutations in yeast Frq1 EF hands did not display a temperature-sensitive phenotype like the quadruple mutant in the frq1-I^{ts} allele, consistent with our observations. By contrast, the triple mutant $Frq^{2,3,4}$ did not bind $^{45}Ca^{2+}$ to a significant extent; hence in HuFrq, EF hand 1 does not constitute a high affinity Ca^{2+}-binding site in HuFrq, as predicted earlier from sequence analysis.

Overall Structure—The crystal structure of HuFrq was solved by the molecular replacement method using neurocalcin

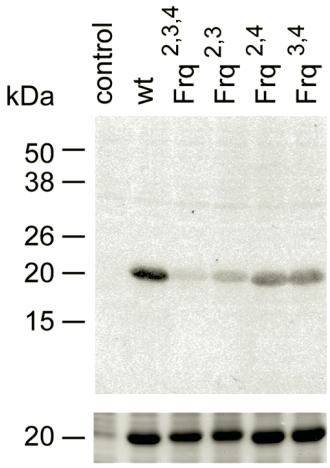

FIG. 3. **Ca^{2+}-binding sites of HuFrq.** $^{45}Ca^{2+}$-binding assay is shown. Bacterial lysates of *E. coli* overexpressing HuFrq (*wt*) or HuFrq mutants E81V/T117A/T165A ($Frq^{2,3,4}$), E8IV/T117A ($Frq^{2,3}$), E81V/T165A ($Frq^{2,4}$), and T117A/T165A ($Frq^{3,4}$) were resolved in 12% polyacrylamide, 0.1% SDS gels. Gels were Coomassie Blue-stained (*bottom*) or blotted in parallel to nitrocellulose for $^{45}Ca^{2+}$ incubation (*top*) as described under "Experimental Procedures." Lysates of *E. coli* transformed with an empty expression vector were used for control.

(14) as a search model and was refined to 1.9 Å resolution. The structure consists of residues Asn^5–Val^{190} with good stereochemistry; clear electron density maps could be observed for all structural elements (Fig. 4*A*). As predicted, HuFrq shares the typical α-helical fold found in homologous proteins, with overall dimensions of 35 × 60 × 40 Å. HuFrq contains 10 helices labeled A to J (Fig. 4*B*). Consistent with the recently proposed NMR-derived model of yeast Frq (29), the four EF hands, which all present the typical architectural short β-strand, come in two pairs: an N-terminal pair (EF1, EF2) and a C-terminal pair (EF3, EF4), which are connected by the hinge loop 93–97 and related by an approximate 2-fold axis. The hinge loop conformation positions the four EF hands on one side of the molecule in a tandem linear array. This structural arrangement is similar to the ones seen in other members of the myristoyl-switch Ca^{2+}-binding proteins, *e.g.* neurocalcin, recoverin, and GCAP (1). It is, however, different from the dumbbell arrangement found in *e.g.* calmodulin and tropinin C (30). The HuFrq structure contains three calcium ions bound to EF hands EF2, EF3, and EF4. The Ca^{2+} coordination in HuFrq is virtually identical to recoverin and neurocalcin. The side chains of residues x, y, and z in the 12-residue loop each provide an oxygen atom, as does the main chain carbonyl of residue y. Two additional oxygen atoms come from the conserved glutamic side chain of residue z and a water molecule.

Structural Comparison with Homologous Proteins—For residues 8–175, the HuFrq overall fold is similar to that of neurocalcin (14) with an r.m.s.d. value of 1.3 Å for 164 Cα atoms (Fig. 4*C*). Extended comparison with the structure of recoverin (31) yields a r.m.s. deviation of 1.7 Å for only 123 Cα atoms. These values indicate that the HuFrq structure is more closely related to that of neurocalcin. This reflects the high sequence identity existing between the two proteins, which is 61% for the whole molecule, compared with only 41% between HuFrq and recoverin. However, whereas neurocalcin dimerizes in solution (14), no dimeric assembly could be observed for HuFrq in concentrated solution or in the crystals (data not shown); this suggests that the distinct oligomeric assembly of these proteins may be related to their biological functions.

Novel Hydrophobic Crevice—The dominant and striking feature of the HuFrq structure is the large positional shift of the C-terminal helix J compared with its position in the recoverin

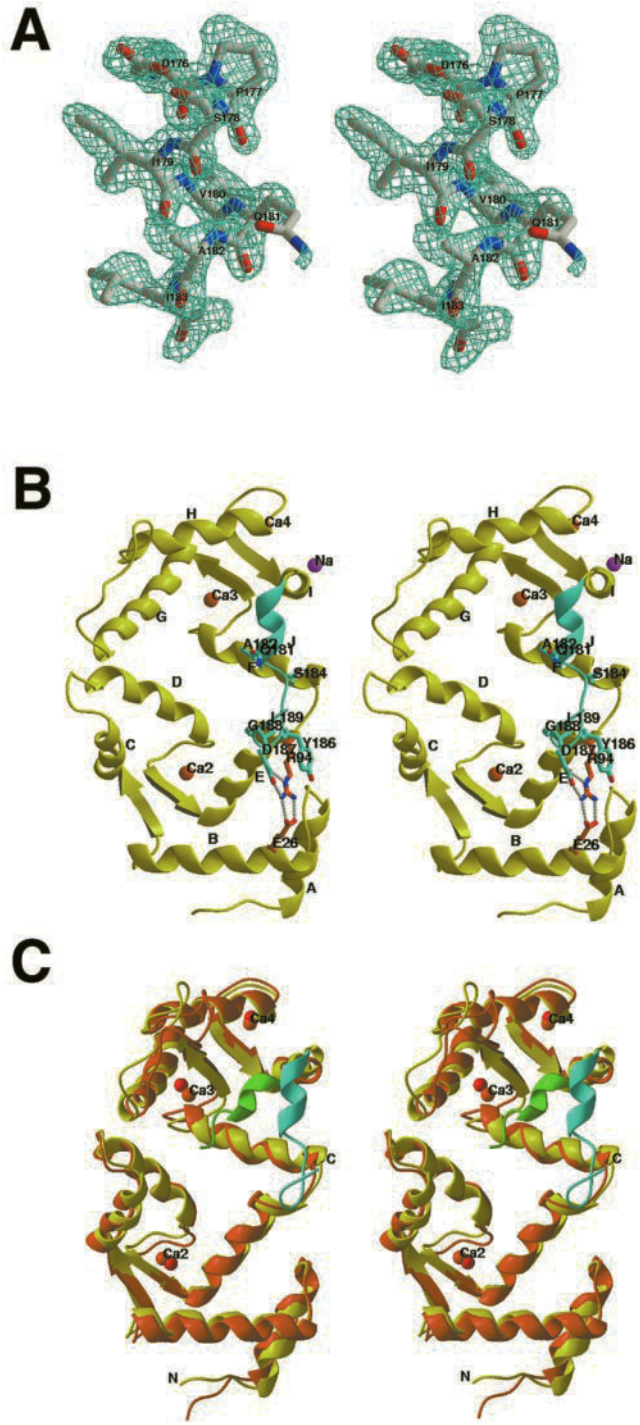

FIG. 4. **Quality of the map and overall fold of HuFrq.** *A,* stereo view of the 1.9 Å resolution omit 2Fo-Fc averaged electron density map, contoured at 1σ, showing part of helix J. The coordinates of this region were omitted and the protein coordinates refined by simulated annealing before the phase calculation. *B,* stereo *ribbon* diagram of HuFrq with bound Na^+ and Ca^{2+} ions. Secondary structure elements are indicated as in Fig. 1. Labels *Ca2*, *Ca3*, and *Ca4* refer to the Ca^{2+} ions bound to EF hands EF2, EF3, and EF4, respectively. Functionally important side-chain residues in the vicinity of helix J are shown as *blue/orange* bonds with *red* oxygen and *blue* nitrogen atoms. Hydrogen bonds are shown as *dotted lines*. *C,* stereo overlay of HuFrq (*yellow/cyan*) and neurocalcin (*orange/green*) oriented as in *B*. Helix J is highlighted in *cyan* for HuFrq and *green* for neurocalcin.

and neurocalcin structures. Indeed, helix J has moved by 45° as a hinge-type rigid-body motion, with the residue pair Asp^{176}-Pro^{177} acting as a pivot point, to adopt an original position that is well ordered in our structure (Fig. 5, *A* and *C*). As a result,

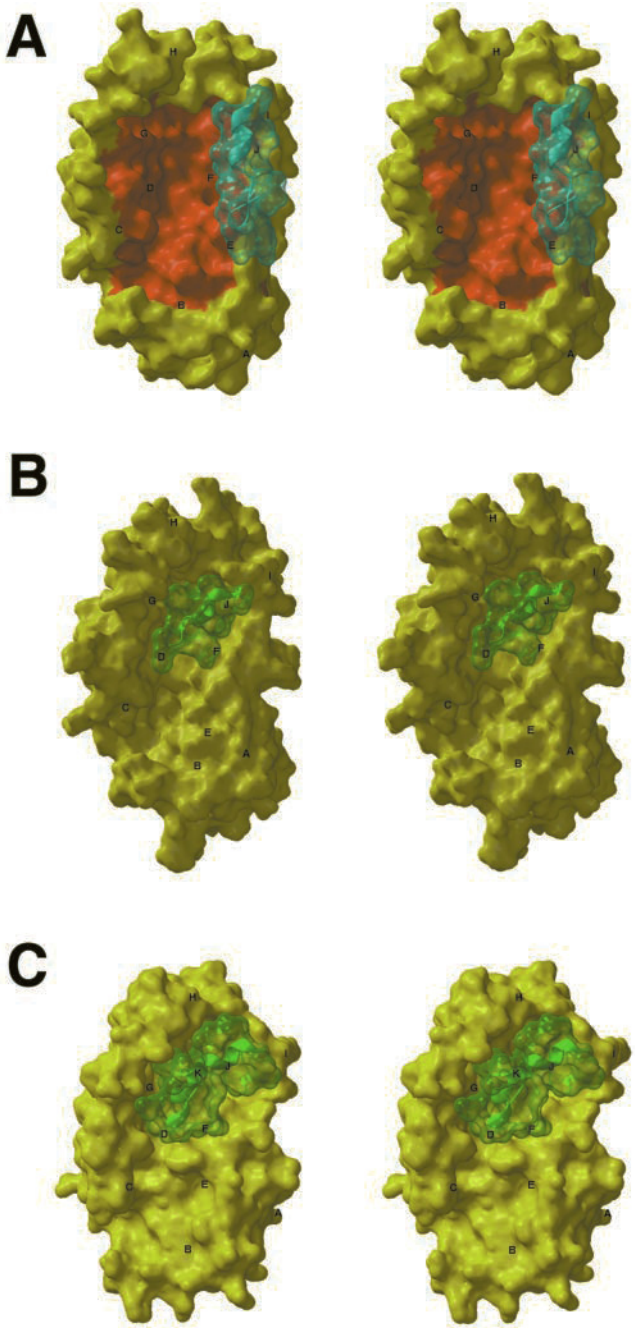

FIG. 5. **Structural differences between HuFrq and homologous proteins.** Molecular surface of HuFrq (*A*), viewed down the large hydrophobic crevice (*orange*) and oriented as in Fig. 2., neurocalcin (*B*) and recoverin (*C*) (same orientation). Secondary structure elements are labeled. The C-terminal helices, helix J in HuFrq (*cyan*) and in neurocalcin (*green*) and helices J and K in recoverin (*green*) are displayed.

the helix is tightly packed against loop αE-αF where it establishes numerous polar and hydrophobic interactions, consistent with an average mobility similar to that of other structural elements in the molecule. As a consequence of helix J motion, a large hydrophobic crevice, with dimensions 30 × 15 × 15 Å, is unmasked on the HuFrq face that is opposite to the four EF hands (Fig. 5*A*). The crevice is made of 46 residues provided by 8 helices, of which helices D, E, and F contribute to the floor of the crevice, helices C, G on one side and helix J on the other side contribute to the walls, and helices H and B contribute to the top and bottom, respectively. Hence, a quarter of the HuFrq molecule contributes to the structure of the crevice.

The major structural significance of the helix J repositioning for ligand binding is obvious from the complete exposure of the hydrophobic surface region. This new conformation dramatically alters the solvent-accessible molecular surface of the molecule when compared with those of neurocalcin or recoverin. In HuFrq, a large patch of hydrophobic residues line the crevice and still are fully accessible to the solvent (Fig. 5*A*), whereas they are sequestered into the neurocalcin and recoverin protein cores (Fig. 5, *B* and *C*). Actually, fragments of the polyethylene glycol used for crystallization are found well ordered within the crevice, where they could mimic an interacting ligand/membrane partner and shield the crevice from the solvent. Presence of the detergent octyl-glucoside was a requisite to solubilize and reduce aggregation of yeast Frq (29). In HuFrq, the unique disordered surface loop, loop 133–137, along with the C-terminal part of helix C that also presents high mobility, are located at the periphery of the crevice and may also play a role upon ligand/membrane recognition.

Is this α-helix conformational shift specific to HuFrq? To our knowledge, such a large positional shift in the C-terminal portion is novel and unique to HuFrq compared with other members of the family and exemplifies how a structurally related fold can exhibit a distinct binding site. Within the crystal asymmetric unit, a sodium ion is bound in the N-cap of helix J and connects residue Ala^{175} in the αI-αJ loop that precedes helix J of one molecule to residues Thr^{17}, Thr^{20}, and Phe^{22} of the second molecule via the carbonyl atoms; however, there is no evidence for an active role of this ion in the α-helical shift. Instead, sequence differences in the C-terminal ends of proteins of the family may explain the conformational features specific to the HuFrq structure. Indeed, seven residues are conserved in the C-terminal region of HuFrq compared with other members: Ala^{182}, Asp^{187}, Gly^{188}, and Leu^{189}, which are exposed at the periphery of the crevice and may have a role for ligand recognition, and Ser^{184}, Tyr^{186}, and Asp^{187}, which are located on the opposite face where they tightly anchor helix J to the protein core (Fig. 4*B*). A recent report on a yeast Frq model, designed from a combination of partial NMR data and homology modeling based on the recoverin structure, might suggest a similar location of helix J in the yeast homolog (29). Hence, the fact that *Drosophila* Frq possesses a glycine doublet in place of the conserved residue pair Tyr^{186}-Asp^{187} appears most surprising because these substitutions would be expected to destabilize helix J. Finally, a Kv channel-interacting protein has recently been identified as a novel member of the calcium-binding protein family (32), and its C-terminal sequence presents high similarity with the C-terminal region of HuFrq. This suggests that a hydrophobic crevice similar to that found in HuFrq may exist and be involved in the binding of the cytoplasmic N termini of Kv4 α-subunits.

The Calcium Myristoyl Switch—HuFrq may share the molecular mechanisms of calcium-myristoyl switch proteins as seen from the solution structures of recoverin, where the myristoyl group is sequestered in a deep hydrophobic box in the Ca^{2+}-free state (33) and ejected into the solvent to interact with a lipid bilayer membrane in the Ca^{2+}-bound state (34). HuFrq possesses two discrete conformations at the hinge point Lys^{7}-Leu^{8} in the N-terminal region, which therefore is a flexible arm. Residues Gly^{42} and Gly^{96} are the two hinge points that distinguish between the Ca^{2+}-free and Ca^{2+}-bound conformations in recoverin, and these two residues are conserved in HuFrq. Of the five helices that participate in the formation of the myristoyl box in recoverin, four (helices B, C, E, and F), line the large crevice in HuFrq. In addition, most of the hydrophobic residues that are recruited to accommodate the myristoyl group in recoverin are conserved in HuFrq and are solvent-exposed at the crevice surface. In HuFrq, residue Gly^{96}, which

is one of the two hinge points in recoverin, establishes van der Waals contacts with helix J, suggesting that a conformational shift at this position might modify the position of this helix. Would HuFrq use the same structural switch as seen in recoverin, the shape and/or size of its hydrophobic crevice would be dramatically altered, a modification that could reflect a regulatory mechanism. Further biochemical experiments must await production of myristoylated HuFrq to test this hypothesis, although recent studies suggest that the presence of a N-myristoyl group in yeast Frq does not affect its overall structure whether Ca^{2+} is present or not (29).

Rat Frq, as opposed to recoverin, neurocalcin, and hippocalcin, showed a Ca^{2+}-independent interaction with membranes (35), suggesting that the presence of the hydrophobic crevice, so far a feature unique to the Frq, may account for this difference in calcium dependence. As well, yeast Frq binds to and activates PIK1 in a Ca^{2+}-independent manner (6), a feature also consistent with our proposal of the hydrophobic crevice as a functionally important binding site. In contrast, the Ca^{2+}-enhanced interaction of yeast Frq with membranes (29) would suggest that in Ca^{2+}-free yeast Frq the shape of the hydrophobic crevice might be altered.

In summary, we have cloned HuFrq from human cDNA and analyzed its cellular localization in COS cells. HuFrq was overexpressed in *E. coli*, purified to homogeneity, and crystallized in the Ca^{2+}-bound state. This Ca^{2+}-bound HuFrq structure is a critical step toward identification of a physiological protein partner using biological experiments. Further crystallographic investigations will help identify the interactions involved in complex formation and conformation.

Acknowledgment—We thank the European Synchroton Radiation Facility staff for technical support in data collection.

REFERENCES

1. Polans, A., Baehr, W., and Palczewski, K. (1996) *Trends Neurosci.* **19,** 547–554
2. Dizhoor, A. M., Lowe, D. G., Olshevskaya, E. V., Laura, R. P., and Hurley, J. B. (1994) *Neuron* **12,** 1345–1352
3. Chen, C. K., Inglese, J., Lefkowitz, R. J., and Hurley, J. B. (1995) *J. Biol. Chem.* **270,** 18060–18066
4. Pongs, O., Lindemeir, J., Zhu, X. R., Engelkamp, D., Krah-Jentsens, I., Lambrecht, H. G., Koch, K. W., Schwemer, J., and Rivosecchi, R. (1993) *Neuron* **11,** 15–28
5. McFerran, B., Graham, M. E., and Burgoyne, R. D. (1998) *J. Biol. Chem.* **273,** 22768–22772
6. Hendricks, K. B., Wang, B. Q., Schnieders, E. A., and Thorner, J. (1999) *Nat. Cell Biol.* **1,** 234–241
7. Audhya, A., Foti, M., and Emr, S. D. (2000) *Mol. Biol. Cell* **11,** 2673–2689
8. Walch-Solimena, C., and Novick, P. (1999) *Nat. Cell Biol.* **1,** 523–525
9. Godi, A., Pertile, P., Meyers, R., Marra, P., Di, T.ullio, G., Iurisci, C., Luini, A., Corda, D., and De, Matteis, M. A. (1999) *Nat. Cell Biol.* **1,** 280–287
10. Maruyama, K., Mikawa, T., and Ebashi, S. (1984) *J. Biochem.* (*Tokyo*) **95,** 511–519
11. Lindemeier, J. (1995) Flup and flics. Zwei neue Frequenin-verwaudte, an der Signal transduktion beteiligte Ca^{2+}-Bindende Proteine Thesis, Freie Universität Berlin, Germany
12. Otwinowski, Z., and Minor, W. (1997) *Methods Enzymol.* **276,** 307–326
13. CCP4. (1994) *Acta Crystallogr. Sect. D* **50,** 760
14. Vijay-Kumar, S., and Kumar, V. D. (1999) *Nat. Struct. Biol.* **6,** 80–88
15. Navaza, J. (1994) *Acta Crystallogr. Sect. A* **50,** 157–163
16. Brünger, A. T., Adams, P. D., Clore, G. M., DeLano, W. L., Gros, P., Grosse-Kunstleve, R. W., Jiang, J. S., Kuszewski, J., Nilges, M., Pannu, N. S., Read, R. J., Rice, L. M., Simonson, T., and Warren, G. L. (1998) *Acta Crystallogr. Sect. D* **54,** 905–921
17. Roussel, A., and Cambillau, C. (1991) *Silicon Graphics Geometry Partners Directory*, p. 81, Silicon Graphics Corp, Mountain View, CA
18. Laskowski, R., MacArthur, M., Moss, D., and Thornton, J. (1993) *J. Appl. Crystallogr.* **26,** 91–97
19. Barton, G. J. (1993) *Prot. Eng.* **6,** 37–40
20. Christopher, J. A. (1998) The Center for Macromolecular Design, Texas A&M University, College Station, TX
21. Merritt, E. A., and Murphy, M. E. P. (1994) *J. Appl. Crystallogr.* **50,** 869–873
22. Hauenschild, A. (1997) *Frequenin: Untersuchungen zur Struktur and Funktion eines neuronalen Proteins*, Auflage, Wissenschaft and Technik-Verlag, Berlin
23. Olafsson, P., Soares, H. D., Herzog, K. H., Wang, T., Morgan, J. I., and Lu, B. (1997) *Brain Res. Mol. Brain Res.* **44,** 73–81
24. Towler, D. A., Gordon, J. I., Adams, S. P., and Glaser, L. (1988) *Annu. Rev. Biochem.* **57,** 69–99
25. Olafsson, P., Wang, T., and Lu, B. (1995) *Proc. Natl. Acad. Sci. U. S. A.* **92,** 8001–8005
26. Wong, K., and Cantley, L. C. (1994) *J. Biol. Chem.* **269,** 28878–28884
27. Robinson, M. S., and Kreis, T. E. (1994) *Cell* **69,** 129–138
28. Wong, K., Meyers, R., and Cantley, L. C. (1997) *J. Biol. Chem.* **272,** 13236–13241
29. Ames, J. B., Hendricks, K. B., Strahl, T., Huttner, I. G., Hamasaki, N. & Thorner, J. (2000) *Biochemistry* **39,** 12149–12161
30. Yap, K. L., Ames, J. B., Swindelles, M. B., and Ikura, M. (1999) *Proteins* **37,** 499–507
31. Flaherty, K. M., Zozulya, S., Stryer, L., and McKay, D. B. (1993) *Cell* **75,** 709–716
32. An, W. F., Bowlby, M. R., Betty, M., Cao, J., Ling, H.-P., Mendoza, G., Hinson, J. W., Mattsson, K. I., Strassle, B. W., Trimmer, J. S., and Rhodes, K. J. (2000) *Nature* **403,** 553–556
33. Tanaka, T., Ames, J. B., Harvey, T. S., Stryer, L., and Ikura, M. (1995) *Nature* **376,** 444–447
34. Ames, J. B., Ishima, R., Tanaka, T., Gordon, J. I., Stryer, L., and Ikura, M. (1997) *Nature* **389,** 198–202
35. McFerran, B. W., Weiss, J. L., and Burgoyne, R. D. (1999) *J. Biol. Chem.* **274,** 30258–30265